Progress In Electromagnetics Research M, Vol. 82, 61–71, 2019

Plane Wave Scattering by Patches Periodically Placed on a Dielectric Rod Surface

Alexander Ye. Svezhentsev[1, *], Valeriy A. Kizka[2], and Guy A. E. Vandenbosch[3]

Abstract—Plane wave diffraction by a finite number of metal cylindrical rectangular strips (patches) periodically placed on a dielectric rod (DR) surface in azimuth direction is considered. The problem is solved by the Method of Moments (MoM) in the spectral domain using Piece Wise Sinusoidal (PWS) basis functions. Topologies with a highly resonant behavior of the patch currents in both azimuth and longitudinal directions are considered. This includes topologies with 1, 2, or 3 patches that are nearly touching, in which case one can also view the topology as a slotted metal cylinder. For these slotted cylinders with one and two slots it is shown that 2D approximate analytical solutions based on the rigorous Riemann-Hilbert approach yield a good agreement with 3D MoM solutions for the natural frequency of the half wavelength resonance until the slot width reaches 40°. It is found that in the 3D case the natural frequency of the half-wavelength resonance for gap coupled patches tends to zero when the slot is vanishing. The radar cross-section versus frequency, resonant current distributions on the patches and far fields are presented.

1. INTRODUCTION

The topology with metal cylindrical rectangular strips (patches) on a circular dielectric rod (DR) surface can be used in different applications. For example, it can serve as a capacitor in different types of sensing and measurement applications, where it can be used to measure the capacitance between two or more conductors [1]. When the patches are made of noble metals (silver, gold) the topology can be used in cylindrically conformal nanoantennas [2]. The energy concentration in restricted areas, so much required in this research field, can be realized at the resonant frequencies.

In the far past, a similar 2D problem was rigorously solved by the Riemann-Hilbert method. In this case the patches were infinitely long in z-direction and the structure was excited by an electron beam moving along the circle [3]. A detailed analysis of the 2D spectral problem for a slotted circular cylinder with one and two slots, symmetrically located, using above mentioned rigorous approach was presented in [4, 5].

The goal of this paper is to find the resonant behavior of topologies consisting of a finite number of patches periodically placed on the DR surface in the azimuth direction. A plane wave is used as excitation. The problem is solved with the Method of Moments (MoM), using Galerkin's scheme, realized in the spectral domain using PWS basis functions. In [6–8] a similar approach was applied to a cylindrical conformal antenna problem with patches of complex shape. There, the solution efficiency was improved by extracting the asymptotical behavior of the spectral Green's function (GF) in the spectral domain, and adding the spatial equivalent in the spatial domain. A similar approach was followed to

Received 9 March 2019, Accepted 9 June 2019, Scheduled 21 June 2019

* Corresponding author: Alexander Yevgenovych Svezhentsev (oleksandr.svezhentsev@gmail.com).

[1] O.Ya. Usikov Institute for Radiophysics and Electronics, National Academy of Sciences of the Ukraine, 12, Acad. Proskury str, Kharkiv 61085, Ukraine. [2] Faculty of Physics, V. N. Karazin Kharkiv National University, Kharkov, Maydan Svobody 4, Kharkiv 61000, Ukraine. [3] Katholieke Universiteit Leuven, Div. ESAT-TELEMIC, Kasteelpark Arenberg 10, Leuven B-3001, Belgium.

compensate for the surface wave poles in the spectral GF [6–8]. We adopt these techniques also in this paper.

This paper presents the numerical investigation of the radar cross section (RCS) versus frequency for different configurations. Comparisons between 2D and 3D solutions in terms of resonant frequencies versus slot width are given. Current distributions and far field patterns are plotted at the resonant frequencies for different plane wave orientations.

2. PROBLEM FORMULATION AND SOLUTION

The structure under investigation is shown in Fig. 1. Consider an infinitely long dielectric cylinder or rod (DR) of relative permittivity ε_r with radius r_0. A finite number of patches N is conformally placed on the DR surface in azimuth direction. Their dimension in z-direction is W_z. Note that when the slots between the patches are small the structure can be seen as a gap-coupled patch configuration.

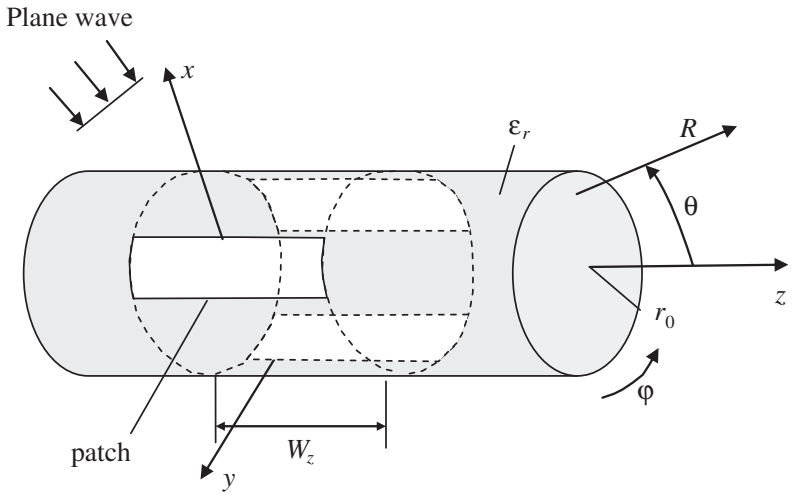

Figure 1. DR with patches periodically placed in azimuth direction.

Omitting all time dependencies $e^{i\omega t}$, let the plane wave be

$$\vec{E}^{inc} = \vec{E}^0 \exp\left(-ik_0(\vec{n}\vec{R})\right) \tag{1}$$

coming from infinity in $\vec{n}$ direction, as shown in Fig. 2. In Eq. (1) $k_0 = 2\pi/\lambda_0$, where λ_0 is the free space wavelength.

The direction $\vec{n}$ can be expressed in a spherical coordinate system, yielding the angles α and β. The angle between the $\vec{E}^{inc}$ vector and the z-axis is γ [6, 7]. Since in this paper we only consider normally incident plane waves with $\alpha = 90°$, $\gamma = 0°$ corresponds with an E-polarized wave ($E_z \neq 0$, $H_z = 0$), and $\gamma = 90°$ corresponds with an H-polarized wave ($H_z \neq 0$, $E_z = 0$).

To find the unknown current distribution on the patches we need to solve the integral equation [6, 7]

$$\mathbf{E}_s^{0,exc}(r_0, z, \varphi) + \mathbf{E}_s^J(r_0, z, \varphi) = 0, \tag{2}$$

where $s = (z, \varphi)$, $\mathbf{E}_s^{0,exc}(r_0, z, \varphi)$ is the excitation field produced by the plane wave, and $\mathbf{E}_s^J(r_0, z, \varphi)$ is the field produced by the patch current $\mathbf{J}^e_{z,\varphi}(r_0, \varphi', z')$ [9], which can be expressed as

$$\mathbf{E}_s^J(r_0, \varphi', z') = \int_{z'} \int_{\varphi'} \begin{bmatrix} \mathbf{J}^e_z(r_0, \varphi', z') \\ \mathbf{J}^e_\varphi(r_0, \varphi', z') \end{bmatrix} \widehat{\mathbf{G}}^J(r_0, r_0, z, z', \varphi, \varphi') dS', \tag{3}$$

where $\widehat{\mathbf{G}}^J(r_0, r_0, z, z', \varphi, \varphi')$ is the Green's function in the spatial domain, and S' is the total patch surface. This integral equation can be solved by using the moment method with Galerkin's scheme

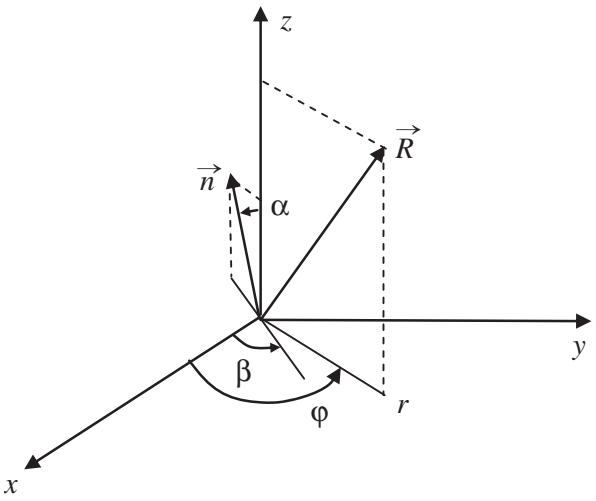

Figure 2. Plane wave orientation angles.

applied in the spectral domain. In this scheme the surface current is first expanded in basis functions as [6–8]

$$\mathbf{J}_s = \sum_{q=1}^{NB} \alpha_q \mathbf{J}_{qs}^b, \tag{4}$$

where α_q are the unknown amplitudes of the basis functions; $\mathbf{J}_{qs}^b$ are the basis functions (PWS); and NB is the total number of basis functions. The moment method transforms the integral equation (2) into a system of linear algebraic equations (SLAE) [6, 7]

$$\mathbf{Z}\boldsymbol{\alpha} = \mathbf{V} \tag{5}$$

where $\boldsymbol{\alpha}[i] = \alpha_i$. $\mathbf{Z}$ is the impedance matrix evaluated in the spectral domain as

$$Z_{ik} = \frac{1}{4\pi^2} \sum_{n=-\infty}^{\infty} \int_{h=-\infty}^{\infty} \widetilde{\mathbf{J}}_i^t(r_0, -n, -h) \widetilde{\widehat{\mathbf{G}}}^J(r_0, n, h) \widetilde{\mathbf{J}}_k^b(r_0, n, h) dh, \tag{6}$$

where $\widetilde{\widehat{\mathbf{G}}}^J(r_0, n, h)$, $\widetilde{\mathbf{J}}^b(r_0, n, h)$, and $\widetilde{\mathbf{J}}^t(r_0, -n, -h)$ are the Fourier transforms (FT) of $\widehat{\mathbf{G}}^J$, $\mathbf{J}_{qs}^b$, and $\mathbf{J}_{qs}^t$, respectively, with $\mathbf{J}_{qs}^t$ being the test function. The spectral Green's function $\widetilde{\widehat{\mathbf{G}}}^J(r_0, n, h)$ components are available in Appendix A (see Eq. (A1)). To speed up the calculations in Eq. (6) the spectral GF asymptotes were extracted in the spectral domain and added again in the spatial domain, as in [6–8]. Note that the principal terms of these spectral asymptotes are the same as in [6–8]. In Eq. (5) the elements of the voltage column vector $\mathbf{V}$ are calculated in the spatial domain as

$$V_i^s = -\iint_{S_i} ds' \mathbf{J}_{is}^t \mathbf{E}_s^{0,exc}(r_0, z, \varphi), \tag{7}$$

where S_i is the surface of the ith basis function. The spectral components of the excitation field are presented in Appendix A (see Eqs. (A2)–(A3)). The Fourier transforms of the basis functions and the final formulas for the calculation of the elements V_i^s can be found in Appendix C of [6].

Using the solution of Eq. (5) and working out the approximation of the scattered field in Eq. (3) in the far zone [10], the far field $\mathbf{E}_s^J(r_0, z, \varphi)$ can be presented as a spherical wave $\mathbf{E}^{\cdot J}(R, \theta, \varphi)$. Then the RCS can be evaluated as

$$\sigma_{uv} = \frac{4\pi \left| \mathbf{E}^J \left(R, \theta = \pi/2, \varphi = \beta \right) \cdot \mathbf{v} \right|^2}{\left| \mathbf{E}_u^0 \right|^2}, \tag{8}$$

where $u = (z, \varphi)$, $\mathbf{E}^J \cdot \mathbf{v}$ is the v-component ($v = (\theta, \varphi)$) of the scattered field in the direction reverse to the plane wave arrival, i.e., in the $-\mathbf{n}$ direction. In Eq. (8), u and v stand for the vector component considered for the incident plane wave field and scattered field, respectively.

3. PHYSICAL ASPECTS OF THE HALF-WAVELENGTH RESONANCE OF THE HELMHOLTZ TYPE IN THE INFINITE SLOTTED CYLINDER

In this section the physical link between the modes in a 2D infinite circular metal cylinder with one or two slots and the modes in the structure as defined in the previous section is explained. A detailed study of the 2D infinite circular metal cylinder is given in [3–5]. The cylinder without slots, see Fig. 3(a), essentially yields a 2D (Neumann) boundary value problem. The solution of this problem yields a resonant wave number k_{res} ($k_{res} = 2\pi/\lambda_{res}$) that starts with $k_{res} = 0$ for the static case, having a z-component of the magnetic field $H_z = 0$. Formally this mode can be introduced as H_{00}.

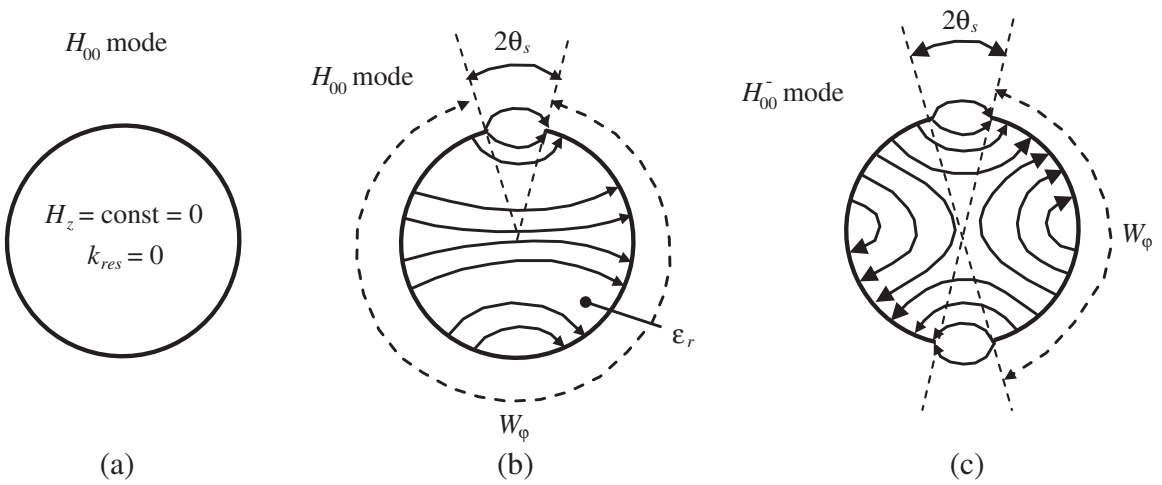

Figure 3. Cross-section of the 2D infinite cylinder: (a) without slots, (b) with one longitudinal slot, (c) with two symmetrically positioned longitudinal slots. The transverse electric field force lines are shown schematically for the lowest H_{00} mode.

However, when a slot with a very small angular width $2\theta_s$ is introduced, see Fig. 3(b), the H_{00} mode is a real mode, with a resonant field and a wave number that are non-zero, namely [3–5]:

$$k_{res} r_0 \sim \ln^{-\frac{1}{2}}(\theta_s), \quad \theta_s \ll 1, \tag{9}$$

In the case of a cylinder with two symmetrical slots, see Fig. 3(c), a polarization degeneration occurs, and two modes H_{00}^+ and H_{00}^- appear in the mode spectrum instead of one H_{00} mode. The lowest one is the H_{00}^- mode whose transverse electric field distribution is shown in Fig. 3(c). Note that formula (9) stays valid also in the case of two slots.

Physically, the emergence of non-zero H_{00} modes is associated with the appearance of the so-called half-wave length resonance, which in the case $\theta_s \ll 1$ is low frequency and thus quasi-static, that is,

$$k_{res} \to 0 \text{ when } \theta_s \to 0. \tag{10}$$

Note that the term "half-wave length resonance" was not used in [3–5]. Instead the resonance was called "slotted resonance", which is not quite correct, since the resonance is related to the size W_φ, and not to the size of the slot.

The infinite metal cylinder with one longitudinal slot has an equivalent in acoustics: a volume cavity with a hole [3–5, 11]. In acoustics, the so-called Helmholtz resonance is found. It is very instructive to see that in electromagnetics for a metal sphere with a hole the low-frequency analogue of the Helmholtz resonance does not exist [4]. One of the goals of this article is to answer the question whether there are low-frequency half-wave length resonances in the 3D case when the metal cylinder is finite, i.e., formed by finite patches on the surface of a circular DR.

4. RESULTS

Consider the situation with one slotted cylinder ($N = 1$) with dimensions W_z and W_φ in z- and φ-direction, respectively, and slot width $2\theta_s$ (see Fig. 4). First we discuss how the RCS depends on frequency for the structural parameters: $r_0 = 2.1\,\text{cm}$, $W_z = 5.95\,\text{cm}$, $W_\varphi = 2r_0(\pi - \theta_s)$, $\varepsilon_r = 2.25$. The patch was meshed into 15×36 segments, which corresponds to $NBz = 504$ and $NB\varphi = 525$, where NBz and $NB\varphi$ are the number of z and φ-directed basis functions, respectively. We consider normal incidence along the x-axis, i.e., $\alpha = 90°$ and $\beta = 0°$, with $\gamma = 45°$ to observe both polarizations at the same time. For $\theta_s = 10°$ the results of the 3D MoM calculations are presented in Fig. 5(a) in terms of the $\sigma_{\varphi\varphi}$ (curve 1) and $\sigma_{z\theta}$ (curve 2) versus frequency. The peak of the curve 1 in Fig. 5(a) corresponds to the resonant frequency $f_{res} = 0.81\,\text{GHz}$ of the principal half wavelength resonance. It is seen that the $\sigma_{\varphi\varphi}$ dependence has a clear peak whereas the $\sigma_{z\theta}$ curve is quite smooth with a resonance occurring at $f_{res} = 1.35\,\text{GHz}$. This corresponds to the case where the half wavelength fits on the patch in z-direction. The resonant current distributions (modulus) of the J_φ-component and the J_z-component are shown in Fig. 5(b) and Fig. 5(c), respectively.

Varying the slot width θ_s, the resonant frequency versus θ_s is given as curve 1 in Fig. 6. This 3D MoM result will be compared with results obtained with the rigorous 2D model given in [4, 5] and with

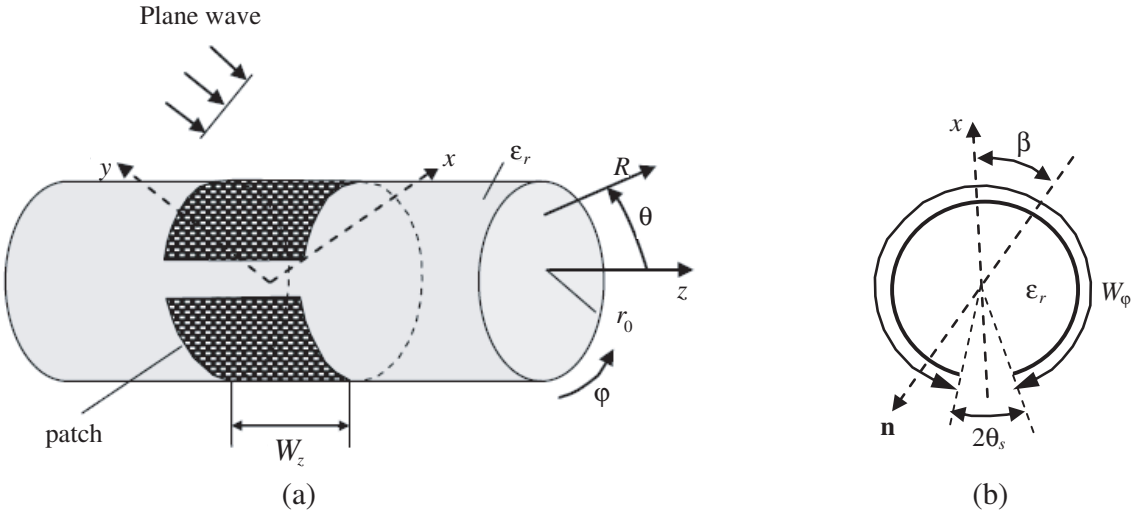

Figure 4. (a) DR with patch in the form of a slotted cylinder, (b) cross-sectional view.

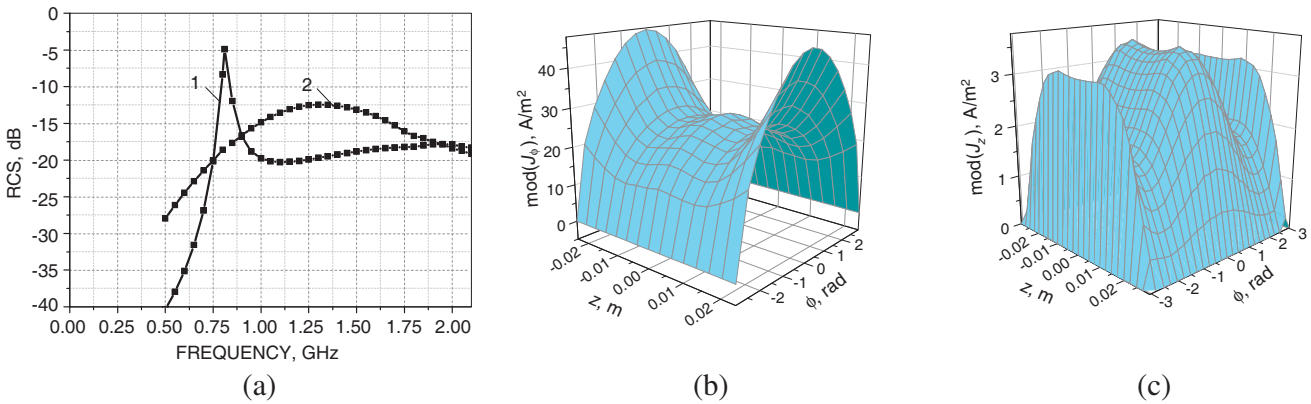

Figure 5. (a) RCS versus frequency, 1 — $\sigma_{\varphi\varphi}$ and 2 — $\sigma_{z\theta}$, for DR with a patch in the form of a slotted cylinder, (b) the amplitude of the J_φ current distribution at the resonant frequency $f_{res} = 0.81\,\text{GHz}$, (c) the amplitude of the J_z current distribution at the resonant frequency $f_{res} = 1.35\,\text{GHz}$.

the simple physical model where the half wavelength in the medium is equal to the patch length.

Modifying the rigorous theory of [4] by taking into account the dielectric filling, the resonant wave number k_{res} of the slotted cylinder obeys the approximate equation for small θ_s values:

$$(\varepsilon_r + 1)(k_{\rm res} r_0)^2 \left[1 + i\pi (k_{res} r_0)^2\right] + \ln^{-1} \sin(\theta_s/2) = 0, \tag{11}$$

which gives an approximate solution for the real part of the resonant frequency

$$f_{res} = \frac{0.3}{2\pi r_0} \left[\frac{-\ln^{-1} \sin(\theta_s/2)}{(\varepsilon_r + 1)}\right]^{1/2} \text{ [GHz]} \tag{12}$$

The same result is obtained by applying the transverse resonance technique to the similar wave guiding problem for the slotted wave as given in [5].

On the other hand, we can apply simple planar patch antenna theory, which tells us that basically the resonant wavelength in the dielectric medium under the patch is twice the patch length in the resonant direction, and thus

$$\lambda_g = 2L \Rightarrow \frac{\lambda_{res}}{\sqrt{\varepsilon_r}} = 2L \Rightarrow f_{res} = \frac{0.3}{\sqrt{\varepsilon_r} 2L} \text{ [GHz]} \tag{13}$$

where λ_g is the wavelength in the medium, and L is the patch size in the resonant direction. In the considered conformal patch case of Eq. (11) can be rewritten as

$$f_{res} = \frac{0.3}{\sqrt{\varepsilon_r} 4 r_0 (\pi - \theta_s)} \text{ [GHz]} \tag{14}$$

The resonant frequencies obtained by formulas (12) and (14) are presented in Fig. 6 as curves 2 and 3, respectively. All geometrical and material parameters remain the same as for Fig. 5.

A comparison of the curves shown in Fig. 6 yields the following. (1) In the range $1° < \theta_s < 20°$ the 3D and 2D solutions demonstrate a good agreement. (2) For the 3D MoM solution with subdomain basis functions it is difficult (large memory, time consuming) to obtain a good result for very small slot widths, namely, $\theta_s < 1°$, unless we considerably increase the number of basis functions. (3) For very small θ_s angles the resonant frequency decreases to zero very fast in accordance with the analytical 2D formula demonstrating the $\ln^{-1}(\theta_s)$ analytical behavior, which, in our opinion, also takes place in 3D case provided that the number of basis functions is sufficient. (4) The approximation (14) does not

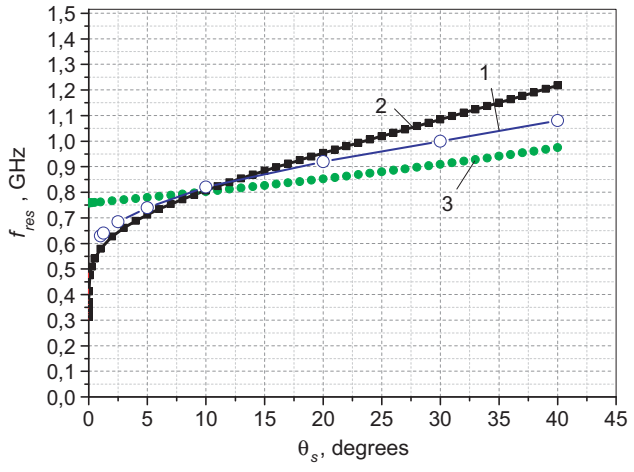

Figure 6. Resonant frequency f_{res} versus half slot width θ_s for the slotted cylinder on the DR surface. 1 — 3D MoM solution (this paper), 2 — 2D rigorous solution, formula (12), and 3 — half wavelength physical model, formula (14).

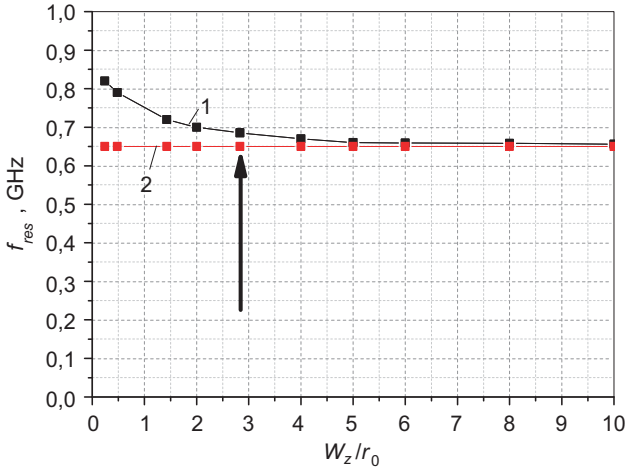

Figure 7. 1 — the resonant frequency f_{res} versus W_z/r_0 for the finite slotted cylinder on the DR surface, 2 — the resonant frequency f_{res} for the infinite slotted cylinder, for both curves $\theta_s = 2.5°$.

work at all for small θ_s because this formula neglects the capacitive coupling between the two almost touching ends.

It is important to note that all calculations in the paper were done for $W_z = 5.95$ cm and $r_0 = 2.1$ cm, namely for the case $W_z/r_0 = 2.833$. A study of the φ-directed resonances when the parameter W_z/r_0 varies is reported in Fig. 7. The resonant frequency (see curve 1) is given versus W_z normalized by r_0 for $\theta_s = 2.5°$. All other parameters, namely, W_φ and ε_r stay the same as in Fig. 6. The curve 2 is the constant line which corresponds to the case of the infinite slotted cylinder (see curve 2 in Fig. 6 for $\theta_s = 2.5°$). In Fig. 6 the line with the arrow indicates the value $W_z/r_0 = 2.833$, which was used in the calculations. Note that for this W_z/r_0 value the difference between curves 1 and 2 is about 5%. To the left of this point the difference becomes bigger (when W_z/r_0 decreases). On the contrary, to the right of this point (when W_z/r_0 increases) the difference becomes smaller and the curve 1 tends to a constant value. Also it was checked that for any W_z/r_0 point of curve 1 a behavior which qualitatively is similar to the curve 1 in Fig. 6 occurs. Namely, whatever the value W_z/r_0 is, the natural frequency of the half-wavelength resonance tends to zero when the slot is vanishing. It is important to note that the resonant frequency behavior discussed in Fig. 7 versus the parameter W_z/r_0 will qualitatively take place for all φ-directed resonances further in this paper.

Consider now the slotted cylinder with two slots. A cross sectional view of a DR with a double slotted cylinder is shown in Fig. 8(a). Modifying the approximation for the natural frequency of a 2D slotted cylinder with two symmetrically located slots given in [4] by taking into account the internal dielectric filling, we obtain the lowest resonance frequency as:

$$f_{res} = \frac{0.3}{2\pi r_0}\left[\frac{-\ln^{-1}\sin(\theta_s)}{(\varepsilon_r+1)/2}\right]^{1/2} \text{ [GHz]} \tag{15}$$

The approximate simple physical half wavelength model for the resonant frequency yields:

$$f_{res} = \frac{0.3}{\sqrt{\varepsilon_r}2r_0(\pi-2\theta_s)} \text{ [GHz]} \tag{16}$$

Results for this double slot case are shown in Fig. 8(b). All geometrical and material parameters remain the same as for the Fig. 5(a), except that now $W_\varphi = r_0(\pi - 2\theta_s)$. Curve 1 corresponds to the 3D MoM calculations, curves 2 and 3 correspond to the 2D analytical approximation by formula (15) and the simple physical model (16), respectively.

It is seen that the 2D model in Eq. (15) and the 3D (MoM) model give similar results for $\theta_s < 20°$. The simple physical model (16) does not work at all for small angles θ_s for the same reason as before,

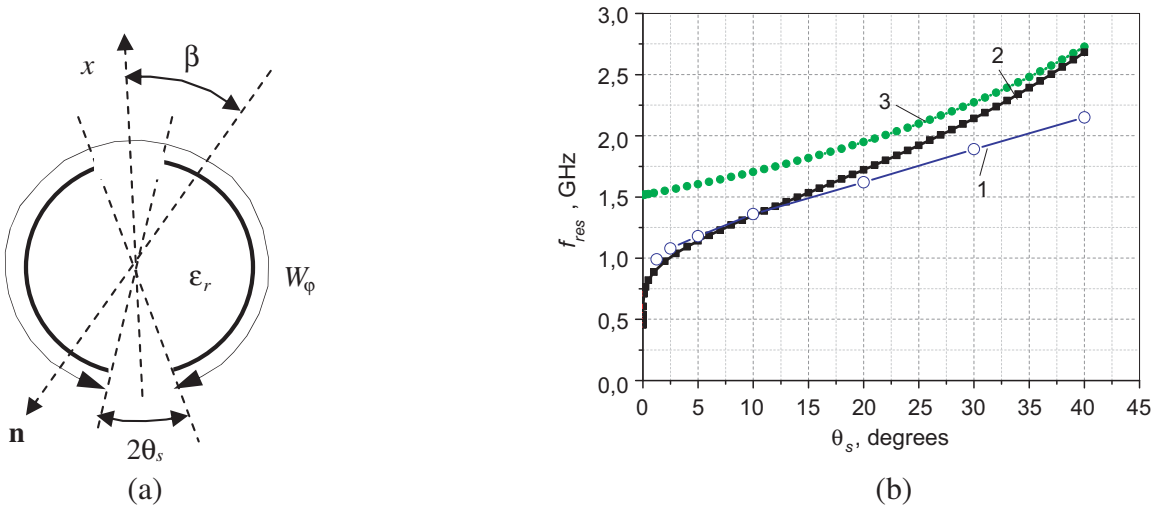

Figure 8. (a) Cross section of DR with double slotted cylinder, (b) resonant frequency f_{res} versus slot half width θ_s for the slotted cylinder with two slots on the DR surface. 1 — 3D MoM solution (this paper), 2 — 2D rigorous solution, formula (15), and 3 — simple physical model, formula (16).

namely, the capacitive gap coupling is not included. The analytical 2D solution gives a $\ln^{-1/2}(\theta_s)$ behavior for very small θ_s, which, in our opinion would also be obtained in the limit in the 3D case for a sufficient number of basis functions in the z direction.

The amplitude and phase of the J_φ component at resonance are shown in Fig. 9(a) and Fig. 9(b), respectively. It is seen from Fig. 9(b) that both patches are excited in phase.

The curves in Fig. 6 and Fig. 8(b), respectively, show that the resonant frequency behavior is rather smooth for all θ_s, except for $\theta_s \ll 1$ where the resonant frequency sharply goes to zero. Physically this means that for $\theta_s \ll 1$ the half wavelength resonance behaves in very special way, namely, $f_{res} \to 0$ when $\theta_s \to 0$. Thus this resonance becomes extremely low frequency and quasi static. This can be explained by the fact that due to the almost touching ends the capacitance tends to infinity when $\theta_s \to 0$ [3–5]. That is why the resonant frequency goes to zero. Note that the half wavelength resonance will disappear in the case $\theta_s = 0$. In this sense this is a singular behavior. Therefore, physically, the behavior $f_{res} \to 0$ when $\theta_s \to 0$ is a property that the half wavelength resonance additionally acquires in the case of small slot width.

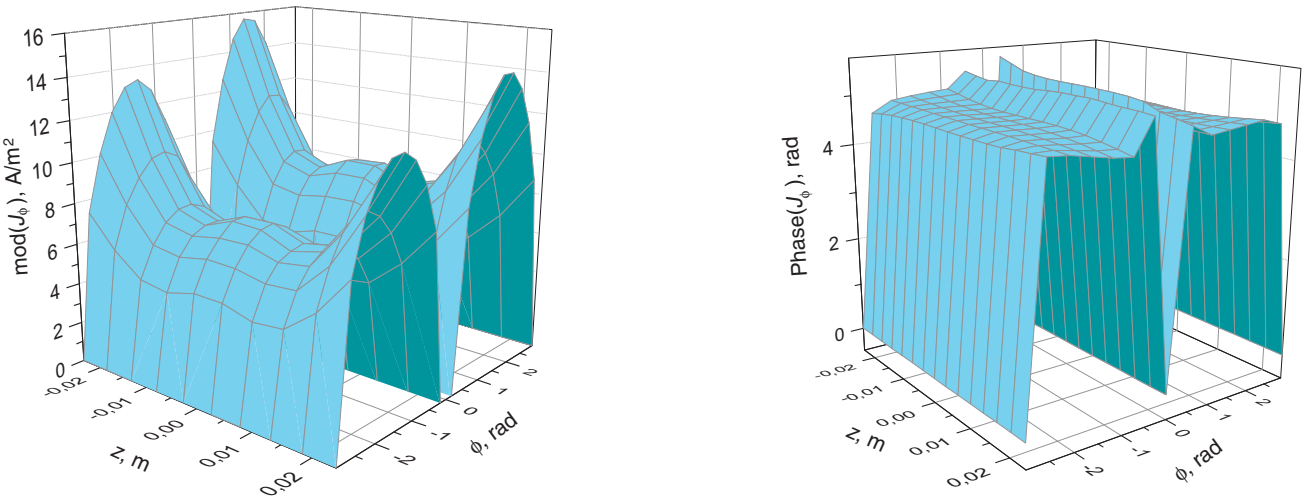

Figure 9. (a) Amplitude and (b) phase of the J_φ component of the current at resonance $f = 1.35$ GHz.

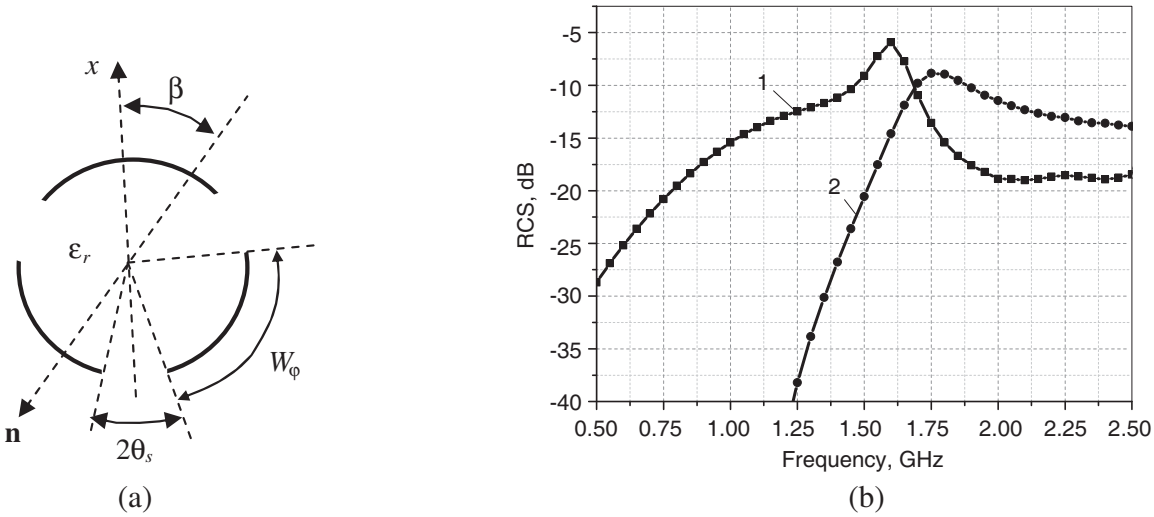

Figure 10. Triple slot cylinder: (a) cross section of DR, (b) RCS versus frequency, 1 — $\sigma_{z\theta}$, 2 — $\sigma_{\varphi\varphi}$.

The last case considered is the DR with a triple slot cylinder (see Fig. 1 for a full view). The slots are symmetrically located, as shown in Fig. 10(a) (cross sectional view). All three slots have the same angular size $2\theta_s$. The other geometrical and material parameters are the same as in the previous cases. The polarization parameter γ is again equal to 45°. This allows considering both H- and E-polarization at the same time. The RCS versus frequency is presented in Fig. 10(b) for $\theta_s = 10°$ which corresponds to $W_\varphi = 3.665\,\text{cm}$. As in previous cases we observe a $\sigma_{\varphi\varphi}$ resonant behavior (see curve 2) at $f_{res} = 1.75\,\text{GHz}$. However, we also see a σ_{zz} resonant behavior now (see curve 1) at $f_{res} = 1.6\,\text{GHz}$. This corresponds to a half wave length resonance along z-direction (E-polar case).

The modulus of the J_z and J_φ current distributions for the mentioned resonances are shown in Fig. 11(a) and Fig. 11(b), respectively.

In Fig. 11(a) three parts can be observed that correspond to the half wavelength current

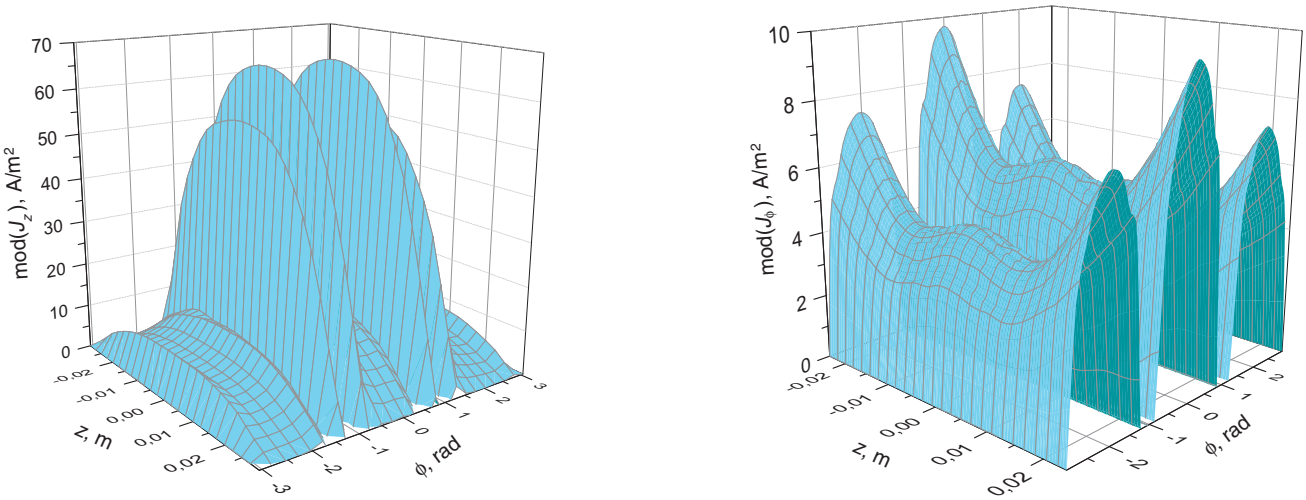

(a) (b)

Figure 11. (a) Amplitude of J_z current distribution at resonance $f_{res} = 1.6\,\text{GHz}$, (b) amplitude of J_φ current distribution at resonance $f_{res} = 1.75\,\text{GHz}$.

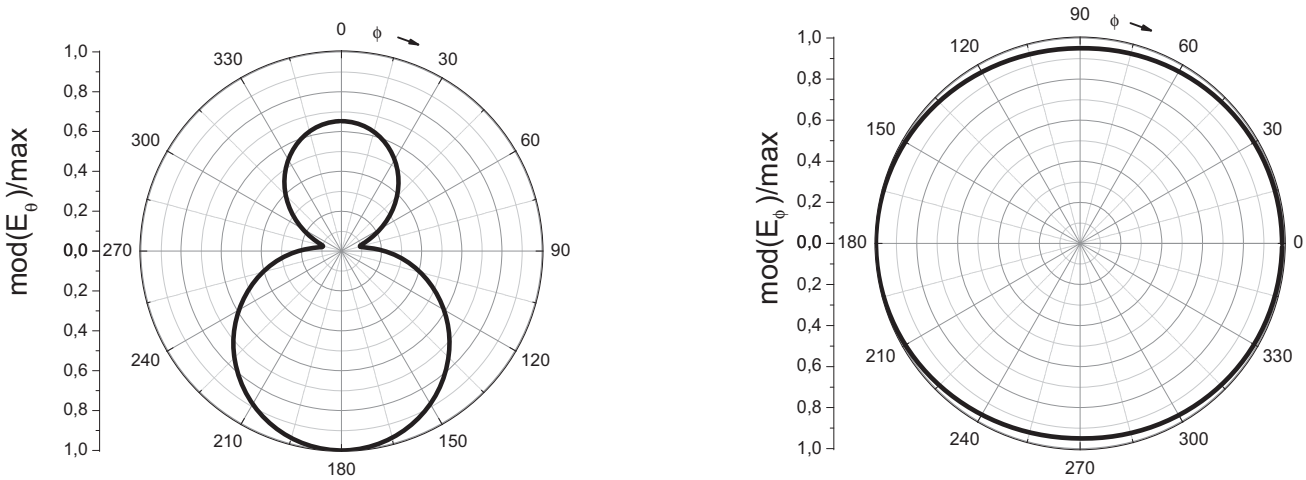

(a) (b)

Figure 12. (a) Radiation pattern E_θ versus φ ($\theta = 90°$) for the E-polar case at the resonant frequency $f_{res} = 1.6\,\text{GHz}$, (b) radiation pattern E_φ versus φ ($\theta = 90°$) for the H-polar case at the resonant frequency $f_{res} = 1.75\,\text{GHz}$.

distributions on the patches along z direction with two gaps in between. On the side edges of the patches you can clearly see jumps which correspond to the J_z current edge singular behavior when the current is parallel to the edge. Similar singular behavior is observed for the J_φ current component in Fig. 11(b). Concerning the phase distributions in Fig. 11, for the J_z current in Fig. 11(a) there is a phase shift π between the middle patch and the side patches, whereas the phase of the J_φ current (see Fig. 11(b)) on all patches remains the same.

Normalized radiation patterns at the $\sigma_{z\theta}$ and $\sigma_{\varphi\varphi}$ resonances 1.6 GHz and 1.75 GHz (see Fig. 10(b)) are presented versus φ in the case $\theta = 90^\circ$ in Fig. 12(a) and Fig. 12(b), respectively.

It is seen from Fig. 12 that in the H-polar case the radiation pattern is omnidirectional whereas in the E-polar case it consists of two unequal beams with maxima at $\theta = 0^\circ$ and $\theta = 180^\circ$.

5. CONCLUSIONS

Plane wave diffraction by a finite number of patches periodically placed on a DR surface in the azimuth direction was discussed. The problem was tackled by solving integral equations with the moment method, using a Galerkin scheme with subdomain PWS basis functions realized in the spectral domain. The resonant regimes were found for different structure configurations. The RCS and resonant frequencies were calculated versus slot width for different plane wave orientations.

We have shown that the resonant behaviors of the structure can be found based on the half wavelength resonances excited in φ direction in a metal cylinder (finite and infinite) with one or two slots. In these cases the presented 3D MoM solution is in good agreement with the approximate analytical 2D Riemann Hilbert method solution for slot widths up to 40°. The difference does not exceed 5% provided that the ratio between patch size in z-direction and DR radius is bigger than 2.833. It was shown that the half wavelength resonance simple model does not work at all in the case of small slot size.

It was found that there is the special behavior of the half wavelength resonance excited in φ-direction for the gap-coupled patches on the DR surface when the gap is vanishing: the resonant frequency also tends to zero. It is crucial to see that in this paper we confirmed the existence of the so-called Helmholtz resonance, as observed in acoustics in a cavity with a hole, also in the 3D electromagnetic case. The half wavelength resonances in both phi-direction (transverse) and z-direction (longitudinal) were observed in the structure with three patches. Resonant current (amplitude and phase) distributions and far field patterns were presented.

APPENDIX A.

A.1. The Spectral Green Functions

The DR with electric sheet currents on its surface can be modeled in a similar way as in [6–8]. The components of the Green function $\widehat{\widehat{\mathbf{G}}}^J(r_0, n, h)$ in the spectral domain, needed in Eq. (6), take the following form:

$$\widehat{\widehat{\mathbf{G}}}^J(r_0, n, h) = \begin{bmatrix} \chi_{nzz}(r_0, \bar{h}) & \chi_{nz\varphi}(r_0, \bar{h}) \\ \chi_{n\varphi z}(r_0, \bar{h}) & \chi_{n\varphi\varphi}(r_0, \bar{h}) \end{bmatrix} \tag{A1}$$

where $\chi_{n(zz)}(r_0, \bar{h})$, $\chi_{n(z\varphi)}(r_0, \bar{h})$, $\chi_{n(\varphi z)}(r_0, \bar{h})$, $\chi_{n(\varphi\varphi)}(r_0, \bar{h})$ are available in [6] (see Appendix A), provided that we put $\Gamma_1 = \overline{\Gamma}_1 = 0$ and as a consequence we come to $F_n(\bar{h}) = \bar{F}_n(\bar{h})$ and $\gamma_{n1}(r, \bar{h}) = \bar{\gamma}_{n1}(r, \bar{h})$ in formula (A1) in [6].

A.2. Evaluation of Excitation Field

The excitation field $\mathbf{E}_s^{0,exc}$ derived as a diffraction problem solution for the plane wave of Eq. (1) incident on the circular dielectric rod, see also [6, 7], takes the form:

$$\mathbf{E}_z^{0,exc}(r, \varphi, z) = \sum_{n=-\infty}^{\infty} \mathrm{d}_{n\,z}(\bar{h}, z) e^{-i\,n(\varphi-\beta)} \tag{A2}$$

$$\mathbf{E}_{\varphi}^{0,exc}(r,\varphi,z) = \sum_{n=-\infty}^{\infty} \mathrm{d}_{n\varphi}(\bar{h},z)e^{-i\,n(\varphi-\beta)} \tag{A3}$$

where $d_{nz}(\bar{h},z)$ and $d_{n\varphi}(\bar{h},z)$ are available in [6] (see Appendix B), taking into account that now $F_n(\bar{h}) = \bar{F}_n(\bar{h})$.

REFERENCES

1. Chen, T., N. Bowler, and J. R. Bowler, "Analysis of arc-electrode capacitive sensors for characterization of dielectric cylindrical rods," *IEEE Transactions on Instrumentation and Measurement*, Vol. 61, No. 1, 233–240, 2012.
2. Svezhentsev, A. Ye., V. Volski, S. Yan, and G. A. E. Vandenbosh, "Shaped nanoantennas on cylindrical and planar substrate," *Proc. of the 2017 IEEE First Ukraine Conference on Electrical and Computer Engineering (UKRCON)*, 650–654, Kiev, Ukraine, May 29–June 2, 2017.
3. Tretyakova, S. S., O. A. Trtyakov, V. G. Sologub, and V. P. Shestopalov, "Excitation of the open structure of the "squirrel cell" type by a charge moving in a circle," *Journal of Technical Physics*, No. 10, 1923–1927, 1967 (in Russian).
4. Shestopalov, V. P., *Summatory Equations in the Modern Theory of Diffraction*, 252, Naukova Dumka, Kiev, 1983.
5. Nosich, A. I. and V. P. Shestopalov, "Excitation of a partially shielded round dielectric rod by lumped sources," *Soviet Physics — Technical Physics*, Vol. 28, No. 12, 1421–1426, 1983.
6. Svezhentsev, A. Ye. and V. V. Kryzhanovskiy, "Patch shape influence upon radar cross section of a cylindrical microstrip antenna," *Progress In Electromagnetic Research B*, Vol. 15, 307–324, 2009.
7. Svezhentsev, A. Ye., V. Kryzhanovskiy, and G. A. E. Vandenbosch, "Cylindrical microstrip array antennas with slotted strip-framed patches," *Progress In Electromagnetic Research*, Vol. 139, 539–558, 2013.
8. Svezhentsev, A. Ye., P. J. Soh, S. Yan, and G. A. E. Vandenbosch, "Green's functions for probe-fed complex-shape cylindrical microstrip antennas," *IEEE Transactions on Antennas and Propagation*, Vol. 63, No. 3, 993–1003, 2015.
9. Schelkunoff, S. A., "Some equivalence theorems of electromagnetics and their application to radiation problems," *Bell Syst. Tech. Journ.*, Vol. 15, 92, 1936.
10. Harrington, R. F., *Time-harmonic Electromagnetic Fields*, McGraw-Hill Book Company, 1961.
11. Helmholtz, H., *Theorie der Luftschwingungen in Rohren mit offenen Enden*, Crelle, 1860.